

Anisotropic Skyrmion and Multi- q Spin Dynamics in Centrosymmetric Gd_2PdSi_3

M. Gomilšek,^{1,2,3,*} T. J. Hicken,^{4,3} M. N. Wilson,^{5,3} K. J. A. Franke,^{6,3} B. M. Huddart,^{7,3} A. Štefančič,⁸ S. J. R. Holt,^{8,†} G. Balakrishnan,⁸ D. A. Mayoh,⁸ M. T. Birch,^{9,10,3} S. H. Moody,^{11,3} H. Luetkens,⁴ Z. Guguchia,⁴ M. T. F. Telling,¹² P. J. Baker,¹² S. J. Clark,³ and T. Lancaster³

¹*Jožef Stefan Institute, Jamova c. 39, SI-1000 Ljubljana, Slovenia*

²*Faculty of Mathematics and Physics, University of Ljubljana, Jadranska u. 19, SI-1000 Ljubljana, Slovenia*

³*Department of Physics, Durham University, South Road, Durham DH1 3LE, United Kingdom*

⁴*Laboratory for Muon Spin Spectroscopy, Paul Scherrer Institut, 5232 Villigen PSI, Switzerland*

⁵*Department of Physics and Physical Oceanography, Memorial University, A1B 3X7, Canada*

⁶*School of Physics and Astronomy, University of Leeds, LS2 9JT, United Kingdom*

⁷*Clarendon Laboratory, University of Oxford, Department of Physics, Oxford OX1 3PU, United Kingdom*

⁸*University of Warwick, Department of Physics, Coventry CV4 7AL, United Kingdom*

⁹*Max Planck Institute for Intelligent Systems, Heisenbergstrasse 3, D-70569 Stuttgart, Germany*

¹⁰*RIKEN Center for Emergent Matter Science, JP-351-0198 Wako, Japan*

¹¹*Laboratory for Neutron Scattering and Imaging,*

Paul Scherrer Institut, 5232 Villigen PSI, Switzerland

¹²*ISIS Facility, STFC Rutherford Appleton Laboratory,*

Didcot, Oxfordshire OX11 0QX, United Kingdom

(Dated: February 4, 2025)

Skyrmions are particle-like vortices of magnetization with non-trivial topology, which are usually stabilized by Dzyaloshinskii–Moriya interactions (DMI) in noncentrosymmetric bulk materials. Exceptions are centrosymmetric Gd- and Eu-based skyrmion-lattice (SkL) hosts with zero DMI, where both the SkL stabilization mechanisms and magnetic ground states remain controversial. We address these here by investigating both the static and dynamical spin properties of the centrosymmetric SkL host Gd_2PdSi_3 using muon spectroscopy (μSR). We find that spin fluctuations in the non-coplanar SkL phase are highly anisotropic, implying that spin anisotropy plays a prominent role in stabilizing this phase. We also observe strongly-anisotropic spin dynamics in the ground-state (IC-1) incommensurate magnetic phase of the material, indicating that it hosts a meron-like multi- q structure. In contrast, the higher-field, coplanar IC-2 phase is found to be single- q with nearly-isotropic spin dynamics.

Topological spin textures can support exotic spin dynamics with a range of potential applications [1, 2]. Especially promising are materials hosting skyrmions, which are topologically-protected, non-coplanar vortices in the magnetization, that behave as extended particles [1, 3]. While in bulk they are usually found in noncentrosymmetric materials and stabilized by Dzyaloshinskii–Moriya interactions (DMI), which select a skyrmion helicity [4], they were also found to be stabilized by competing magnetic interactions in bulk centrosymmetric compounds with no preferred helicity and no net DMI [1, 2]. Examples are Gd_2PdSi_3 , with a triangular spin lattice [5–15], $\text{Gd}_3\text{Ru}_4\text{Al}_{12}$ with a breathing kagome spin lattice [12, 16–18], and GdRu_2Si_2 [19–28], GdRu_2Ge_2 [29], and EuAl_4 [30–32] with tetragonal spin lattices. Common to these highly-symmetric rare-earth materials is that they host incommensurate skyrmion-lattice (SkL) phases with very small (1.9–3.5 nm) skyrmions that are stable under higher applied fields (~ 1 T) and over a wider range of T than their DMI-stabilized counterparts [1, 2].

The stabilization mechanism for these centrosymmetric skyrmions is controversial, with suggestions including: (i) short-range geometrical frustration [17, 33–36], (ii) long-range Ruderman–Kittel–Kasuya–Yosida (RKKY) interactions plus dipolar [10, 14, 22, 24, 26, 37] or bi-

quadratic exchange [21, 27, 29, 38–42], and (iii) competition of orbital-dependent exchange [43, 44]. Most, but not all [38, 39], such scenarios require spin anisotropy. The zero-field (ZF) ground state is also contentious [11], with early studies of Gd_2PdSi_3 suggesting an exotic, triple- q magnetic structure [5, 6] [e.g., a lattice of merons and antimerons (ML), which are half-skyrmion-like spin textures [21, 25, 29, 45]], while recent calculations under scenario (ii) indicated a simpler, single- q helical ground state [10, 37], as found in DMI-stabilized SkL hosts [46]. Investigations of centrosymmetric SkL hosts have focused on their static and topological properties, with less attention [32] paid to emergent spin dynamics [34], which can elucidate both the stabilization mechanism and single- or multi- q structure. Characteristic dynamics of SkL and related spin textures have been observed in a range of DMI-stabilized SkL hosts [1, 2, 47–49]. For accessing these, muon spectroscopy (μSR), a local-probe technique sensitive to spin fluctuations over a unique frequency range (applicable also at low applied fields and to conductive samples) [50], has proven valuable [51–57]. However, the narrow T range of DMI skyrmions [1, 2, 46] limited the ability to extract the underlying spin-wave dispersions unambiguously. Namely, when T is comparable to the transition temperature T_N , spin dynamics can be

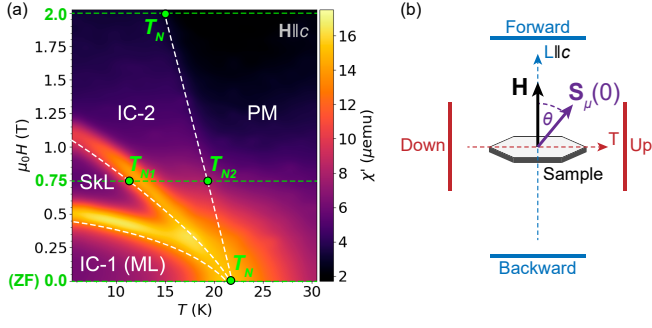


Fig. 1. (a) Real part of AC susceptibility with applied field along the c axis. Phase boundaries (white) and μ SR scans (green) with the corresponding transition temperatures T_N are shown. Phase assignments, including our suggested assignment of the IC-1 phase as a meron–antimeron lattice (ML), combine evidence from a range of techniques [5–7]. (b) Sample and detector arrangement for μ SR measurements. The initial muon spin $\mathbf{S}_\mu(0)$ lies at an angle θ to the applied field $\mathbf{H} \parallel c$, which points along the longitudinal direction L (blue). The transverse direction T (red) lies in the hexagonal ab plane.

come dominated by multi-magnon processes and/or critical fluctuations (usually over $T_N/2 \lesssim T \lesssim 2T_N$), obscuring the underlying spin-wave dispersion.

In this Letter, we investigate the most-studied centrosymmetric SkL host Gd_2PdSi_3 [5] using μ SR and AC susceptibility, complemented by density functional theory (DFT) calculations of muon stopping sites [58]. We find clear signatures of spin reorientation transitions between the incommensurate magnetic phases and reveal the highly anisotropic character of their spin fluctuations. By exploiting the relatively wide region of stability of these phases, we characterize the low-energy dispersion relations of their spin-wave excitations. The excitations in the high-field coplanar incommensurate IC-2 phase are consistent with a single- q fan-like spin texture [5, 6] with nearly-isotropic spin fluctuations. However, in the ground-state ZF incommensurate IC-1 phase, we find that low-energy in-plane (ab -plane) spin fluctuations dominate, while out-of-plane (c -axis) fluctuations are almost completely suppressed. This, combined with previous resonant X-ray scattering (RXS) and resistivity data [5, 6], indicates that the IC-1 phase is a complex, triple- q magnetic structure, not the recently-predicted single- q helical structure [10, 37]. This disfavors SkL-stabilization scenario (ii) above. Finally, in the SkL phase, out-of-plane fluctuations dominate instead, with in-plane fluctuations suppressed as a power-law in T . We, therefore, argue that spin anisotropy is a key ingredient in stabilizing the SkL phase in centrosymmetric rare-earth magnets.

Single crystals of Gd_2PdSi_3 were synthesized, with five high-quality $\approx 9 \text{ mm}^2 \times 0.6 \text{ mm}$ plate-like crystallites with c -axis normals extracted [15, 58]. AC magnetic

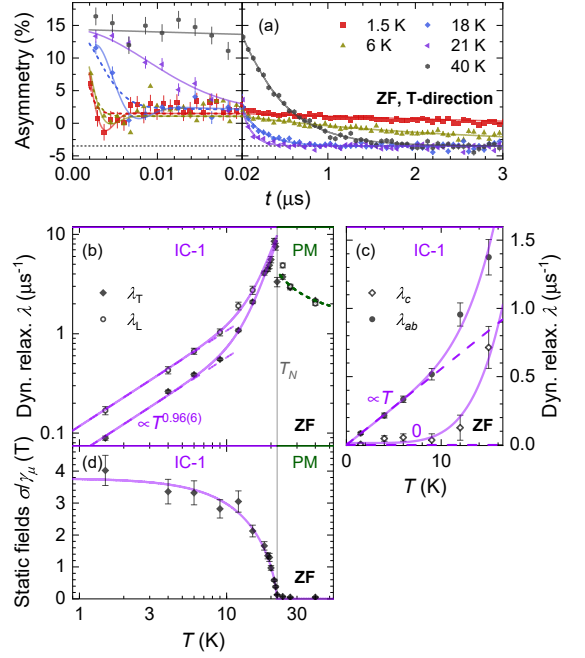


Fig. 2. IC-1 phase in ZF. (a) ab -plane (T -direction) muon asymmetry at early (left) and late times (right). Solid lines on the left panel are guides to the eye; dashed lines are fits using the model described in the text. Horizontal dashed line shows the background level a_{bgd} . (b) Dynamical relaxation rates and (c) contributions to these rates due to out-of-plane (c -axis) and in-plane (ab -plane) spin fluctuations. Solid lines at $T < T_N$ are guides to the eye, which include a critical divergence near T_N (evident as an increase in λ above $\sim 10 \text{ K}$); dashed lines are the single-power-law low- T limits. (d) Quasi-static magnetic fields from T -direction data on panel (a).

susceptibility measurements reproduced the phase diagram from previous studies [5–7], including the SkL phase [Fig. 1(a)]. For μ SR measurements, the crystallites were assembled in a mosaic with coaligned c -axes [58]. The initial muon spin pointed along the out-of-plane (c -axis) direction in longitudinal-field (LF) measurements ($\theta = 0$), and at an angle of $\theta \approx 50^\circ$ from the c axis in ZF and transverse-field (TF) measurements [Fig. 1(b)]. In a μ SR experiment, longitudinal- ($L \parallel c$) and transverse- ($T \perp c$) muon spin components evolve independently [50], producing asymmetries $A_j(t) \propto \langle S_\mu^j(t) \rangle$, where $S_\mu^j(t)$ is the muon spin component j at time t , in detector pairs positioned along directions $j = L$ and T [Fig. 1(b)]. An intermediate value of θ in ZF and TF experiments thus allowed us to track the different impacts of the material’s magnetic state on the time evolution of the L and T muon spin components from a single experimental run. On the other hand, in LF experiments (where $\theta = 0$) only the L muon spin component could be measured. All measurements were made after first zero field cooling (ZFC) the sample to base T , while magnetic fields were always applied along the c -axis, which is an axis of threefold crystallographic symmetry and thus a magnetic eigenaxis.

We first performed μ SR measurements on warming from the IC-1 ground-state of Gd_2PdSi_3 in ZF on the GPS instrument at the Swiss Muon Source ($S\mu S$). At low T , a highly-damped oscillation in the T-direction (ab -plane) muon-spin component was observed at early times $t \ll 0.1 \mu\text{s}$ [Fig. 2(a)] due to a broad distribution of quasi-static local fields at the muon site [58] that originate from long-range incommensurate magnetic ordering of Gd^{3+} spins. At later times, up to $t \approx 10 \mu\text{s}$, a further exponential relaxation was observed due to dynamical fluctuations of Gd^{3+} spins slower than the muon precession frequency [50]. The measured T-direction asymmetry data were fitted using $A(t) = [a_s - a_r]e^{-\sigma^2 t^2} + a_r e^{-\lambda t} + a_{\text{bgd}}$, where $a_s = \text{const.}$ is the total sample asymmetry and $a_{\text{bgd}} = \text{const.}$ is the background due to muons hitting the sample holder. The early-time damping rate σ in this model is proportional to the average strength of quasi-static local magnetic fields at the muon site [58] and is expected to roughly scale with the magnitude of ordered moments in the sample. a_r is the late-time relaxing asymmetry due to the fraction of local fields that initially point along the measured muon spin component [58], and λ is the dynamical relaxation rate due to slow fluctuations of fields orthogonal to the measured muon-spin component [50, 58].

Fit results for the T direction are shown in Fig. 2(b,d) with the transition temperature $T_N = 22(1)$ K consistent with AC susceptibility [Fig. 1(a)]. In the itinerant paramagnetic (PM) regime at $T > T_N$ we find $\sigma \approx 0$. Around $T \approx T_N$, critical spin fluctuations cause λ_T to exhibit a divergence characteristic of a continuous phase transition as we enter the IC-1 phase. In the ordered IC-1 phase ($T < T_N$) the average local-field strength increases and saturates as an order parameter, $\sigma \propto [1 - (T/T_N)^{3/2}]^\beta$ [32, 50] with $\beta = 0.7(1)$, which is large but close to $\beta = 0.50(5)$ found in the centrosymmetric SkL host EuAl_4 in ZF [32]. At low T , slow spin fluctuations cross over into a power-law $\lambda_T \propto T^p$ with $p = 0.96(6)$. A low- T power-law dependence of the dynamical relaxation rate could be understood within spin-wave theory for a two-magnon process, which for a single gapless magnon band predicts [58–60]

$$p = \frac{2D}{s} - 1, \quad (1)$$

where $D \leq 3$ is the (integer) dimensionality of spin-wave excitations and s is the dominant power in their dispersion relation $\omega \propto |\mathbf{q} - \mathbf{q}_0|^s$ around the ordering wave vector \mathbf{q}_0 . Usually, $s = 2$ for ferromagnetic ($\mathbf{q}_0 = 0$) and $s = 1$ for antiferromagnetic and incommensurate states ($\mathbf{q}_0 \neq 0$) [61]. The measured T-direction $p \approx 1$ in the IC-1 phase would thus correspond to a 1D (single- q) magnetic structure ($D = s = 1$), if the single-band approximation were valid.

To test this, we also fitted the L-direction (c -axis) data using the same model to obtain the relaxation rate

λ_L [Fig. 2(b)]. Assuming bulk uniaxial symmetry, we have [50, 58] $\lambda_L = 2\lambda_{ab}$ and $\lambda_T = \lambda_{ab} + \lambda_c$, where λ_{ab} and λ_c are the relaxation contributions due to dynamical fluctuations of in-plane and out-of-plane magnetic fields at the muon site, respectively. At the nearly-symmetric in-plane muon site that we obtain from DFT stopping site calculations (near the centre of a Gd^{3+} triangle) [58], λ_{ab} and λ_c ultimately arise from fluctuations of in-plane and out-of-plane Gd^{3+} spin components, respectively. This can be seen from a symmetry decomposition of long-wavelength Gd^{3+} spin textures under local ab -plane reflections and c -axis rotations (for details, see the SM [58]). Fig. 2(c) shows the extracted λ_{ab} and λ_c . Remarkably, in contrast to the single-magnon-band approximation where we should have $\lambda_{ab} \propto \lambda_c \propto T^p$ (for a proof, applicable also to general single- q states, see the SM [58]), we instead find $\lambda_{ab} \propto T$ but $\lambda_c \approx 0$ in the IC-1 phase. Our first result is, therefore, that the IC-1 phase is not a simple single- q magnetic structure, as was predicted [10, 37]. Instead, there appear to be multiple, highly-anisotropic spin-fluctuation modes in this phase. Such behavior is expected for extended, multi- q spin textures [34, 47], such as the hypothesized ML state [5, 6]. Their predominantly in-plane nature appears consistent with easy-plane anisotropy found in this phase [11].

Next, we turn to the IC-2 and SkL phases. Here, we performed separate μ SR measurements in a TF of 0.75 T on the GPS instrument at $S\mu S$ and a LF of 0.75 T on the HiFi instrument at the STFC-ISIS Facility. We warmed from the low- T SkL to the intermediate IC-2 phase, and finally to the PM phase [Fig. 1(a)]. The late-time data were well described by the same model as for the ZF data, simplified to $A(t) = a_r e^{-\lambda t} + a_{\text{bgd}}$ at late times. From T-direction TF data and L-direction LF data we again extracted in-plane λ_{ab} and out-of-plane λ_c spin-fluctuation contributions.

The resulting relaxation rates are shown in Fig. 3(a) with transition temperatures $T_{N1} = 12(1)$ K and $T_{N2} = 20(1)$ K consistent with AC susceptibility [Fig. 1(a)]. The in-plane relaxation λ_{ab} shows a critical divergence at $T \approx T_{N2}$ due to a continuous transition between the PM and IC-2 phases. In the IC-2 regime ($T_{N1} < T < T_{N2}$) we find nearly-isotropic spin fluctuations with $\lambda_c \approx \lambda_{ab}$. (Fitting these to a gapped model $\propto e^{-\Delta/T}$ also yields the same characteristic energy scales $\Delta = 47(3)$ and $49(3)$ K for λ_c and λ_{ab} , respectively.) Any low- T power-law spin-wave behaviour is masked by near-critical fluctuations and interrupted by a transition to the SkL phase at T_{N1} .

The phase transition at T_{N1} does not show any critical divergence in the muon relaxation rate, only a change of slope, implying that it is first-order, consistent with the topologically-non-trivial nature of the SkL [1, 34]. While nearly-isotropic at T_{N1} , we find that highly-anisotropic spin fluctuations emerge with lowering $T < T_{N1}$, similarly to the IC-1 phase. However, while in the IC-1 phase spin fluctuations were predominantly in-plane ($\lambda_c \ll \lambda_{ab}$)

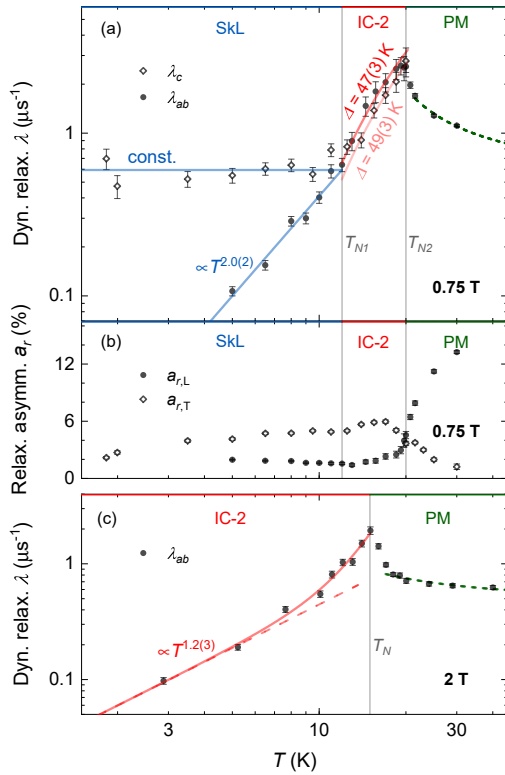


Fig. 3. (a) Contributions to relaxation due to out-of-plane (c -axis) and in-plane (ab -plane) spin fluctuations in the SkL and IC-2 phases in a 0.75 T applied field. (b) Relaxing asymmetry due to quasi-static local fields along the c axis (L) and within the ab plane (T) under these conditions. (c) Relaxation due to in-plane fluctuations in the IC-2 phase in a 2 T field.

the dominant spin fluctuations in the SkL phase are instead out-of-plane, with $\lambda_c \approx \text{const.} \gg \lambda_{ab} \propto T^p$ and $p = 2.0(2)$. We note that $p \approx 2$ would uniquely correspond to $D = 3$, $s = 2$ (3D ferromagnetic) spin excitations under the single-band spin-wave approximation [Eq. (1)], but this is inconsistent with a T -independent λ_c [58]. Instead, there appears to be a large low-energy spin density of states due to multiple spin fluctuation modes, as expected for SkL phases [34, 47–49, 62], that are predominantly polarized out-of-plane (e.g., skyrmion breathing modes [47, 62]).

We next turn to static properties of the SkL and IC-2 phases in an applied field of 0.75 T. Fig. 3(b) shows late-time relaxing asymmetries $a_{r,T}$ and $a_{r,L}$ in the in-plane (T) and out-of-plane (L) directions. Both change rather abruptly at $T \approx T_{N2}$ due to the onset of magnetic order. Assuming bulk uniaxial symmetry we expect [50, 58] $a_{r,T} \propto \langle \hat{B}_a^2 \rangle = \langle \hat{B}_b^2 \rangle$ and $a_{r,L} \propto \langle \hat{B}_c^2 \rangle$, where $\hat{\mathbf{B}} = \mathbf{B}/|\mathbf{B}|$ is the initial direction of a quasi-static local field \mathbf{B} at the muon site. In Fig. 3(b) we see that $a_{r,T}$ exhibits a broad peak in the IC-2 phase at $T_{N1} < T < T_{N2}$, while $a_{r,L}$ exhibits a minimum. These both indicate approximately coplanar quasi-static magnetism in this phase.

In the SkL phase, the difference between $a_{r,T}$ and $a_{r,L}$ becomes smaller, implying that local field directions become more isotropic, as expected for a non-coplanar spin texture [1–3]. Our observation of a coplanar magnetism in the IC-2 phase and non-coplanar magnetism in the SkL phase is consistent with RXS results [5], where this was argued based on the ellipticity of the magnetic moments of individual magnetic Bragg peaks. However, our conclusions are based on a complementary [11], real-space determination of local field directions only accessible to local probes like the muon [50]. Intriguingly, via field-dependent quasi-static μSR measurements, we find that the width of the local field distribution does not scale with the average local field strength in the SkL phase, but does do so in the IC-1 and IC-2 phases (see the SM [58]).

Finally, to assess the low- T dynamics of the IC-2 phase, we performed μSR measurements in a LF of 2 T on the HiFi instrument. The late-time L-direction muon data were well described by the same model as for the 0.75 T data, where the fitted relaxation rate $\lambda_L = 2\lambda_{ab}$ [Fig. 3(c)] shows a transition temperature $T_N = 15(1)$ K consistent with AC susceptibility [Fig. 1(a)]. Near $T \approx T_N$ the muon relaxation rate exhibits a critical divergence characteristic of a continuous phase transition as we enter the IC-2 phase, and at $T < T_N$ it crosses over into a low- T power-law $\lambda_L \propto T^p$ with $p = 1.2(3)$. The observed isotropy of spin fluctuations in this phase [Fig. 3(a)] makes single-band spin-wave theory [Eq. (1)] applicable, with the measured $p \approx 1$ indicating that the IC-2 phase is a 1D (single- q) magnetic structure ($D = s = 1$), as previously suggested [5, 6]. This stands in contrast to multi- q IC-1 and SkL phases found at lower applied fields.

To summarize, our finding of different low- T in-plane and out-of-plane spin fluctuations in both non-coplanar SkL and ground-state IC-1 phases of centrosymmetric Gd_2PdSi_3 contrasts with isotropic fluctuations found in the coplanar single- q IC-2 phase. This should supply a clue to the stabilization mechanism for centrosymmetric skyrmions. In contrast to DMI-stabilized skyrmions [47–49, 62, 63], systematic predictions for SkL spin dynamics for different stabilization-mechanisms are lacking. Nevertheless, it seems unlikely that a spin model without strong intrinsic anisotropy could explain the observed highly-anisotropic SkL and IC-1 spin dynamics. This agrees with suggestions that spin anisotropy [11, 34, 42], combined with long-range interactions, is important for stabilizing the SkL phase [10, 17, 27, 40]. A quantitative determination of the anisotropy of intrinsic magnetic interactions in Gd_2PdSi_3 would thus be crucial [11]. We note that anisotropic magnetic interactions are also found in other representatives of the hexagonal $R_2\text{PdSi}_3$ family (R = rare earth) [64, 65], in the tetragonal centrosymmetric SkL hosts GdRu_2Si_2 and GdRu_2Ge_2 [19, 44, 66–68], and even (weakly) in cubic Gd-based magnets [69]. Furthermore, our observation that the ground-state IC-1 phase is a multi- q magnetic structure (triple- q , based on

previous RXS [5, 6] and neutron-scattering [13] Bragg-peak studies) suggests it is the exotic ML state, as hypothesized in Ref. [5] from RXS and resistivity measurements. While double- q (square-lattice) ML-like states have recently been reported in thin-plate DMI-based $\text{Co}_8\text{Zn}_9\text{Mn}_3$ [45], and bulk tetragonal centrosymmetric GdRu_2Ge_2 [29] and GdRu_2Si_2 [21] (in two phases), the IC-1 phase would be a unique example of a triple- q magnetic ML. Furthermore, the IC-1 phase is the ZF ground state in Gd_2PdSi_3 , while the ML states in $\text{Co}_8\text{Zn}_9\text{Mn}_3$ and GdRu_2Ge_2 are only stabilized under an applied field, and the claimed ZF ML phase in GdRu_2Si_2 has recently been reinterpreted as a topological-charge-stripe state instead [23, 25, 28]. The multi- q nature of the ZF IC-1 phase represents another challenge to theory, as calculations suggested that the ZF state should instead be single- q under the RKKY+dipolar skyrmion stabilization scenario (ii) [10, 37]. Our findings thus disfavour this as the skyrmion stabilization mechanism. Nevertheless, RKKY interactions were found to be strong in the related centrosymmetric SkL host GdRu_2Si_2 via angle-resolved photoemission spectroscopy (ARPES) [24, 26] and quantum-oscillation measurements [22], complemented by *ab initio* calculations [21, 22, 24, 26], so they could still play a role. A very recent ARPES and *ab initio* study of Gd_2PdSi_3 seems to support this [14].

In conclusion, in our muon-spectroscopy study of centrosymmetric Gd_2PdSi_3 we have found large anisotropy in spin dynamics, with qualitatively different behaviour of dominant out-of-plane and subdominant in-plane spin fluctuations in the SkL phase. We have also established the meron-like triple- q nature of its incommensurate IC-1 ground state with dominant in-plane, and nearly-absent out-of-plane, fluctuations. The higher-field IC-2 phase was found to be coplanar and single- q with isotropic spin fluctuations. Our results suggest that the enigmatic stabilization mechanism behind SkL phases in centrosymmetric Gd- and Eu-based materials is likely to be intimately related to spin anisotropy, and not solely RKKY+dipolar. Further local-probe studies of these and related centrosymmetric compounds [1, 2, 70, 71] should be informative in exploring this. Studies of anisotropic spin excitations and their dispersions via inelastic neutron scattering [10], and the anisotropy of static spin correlations via RXS, especially on single crystals, would also be valuable. Finally, our μSR methods could also be extended to study low- T spin anisotropy and dynamics of metastable skyrmions in DMI-based SkL hosts [1].

Research data and code presented in this paper are available at <https://dx.doi.org/10.6084/m9.figshare.28024910>.

We thank Martin Klanjšek and Matej Pregelj at the Jožef Stefan Institute, Slovenia for helpful discussions. Parts of the work were carried out at the STFC ISIS Muon Source, United Kingdom and at the Swiss Muon Source, Paul Scherrer Institute, Switzerland and we are

grateful for the provision of beamtime and experimental support. We thank Raymond Fan and Paul Steadman for enabling us to use the Quantum Design MPMS3 at the I10 support laboratory, Diamond Light Source for AC susceptibility measurements. Computing resources were provided by the Durham HPC Hamilton cluster. M.G. acknowledges the financial support of the Slovenian Research and Innovation Agency through Program No. P1-0125 and Projects No. Z1-1852, N1-0148, J1-2461, J1-50008, J1-50012, N1-0345, and N1-0356. We acknowledge the financial support of the Engineering and Physical Sciences Research Council (EPSRC, UK) through Grants No. EP/N032128/1 and EP/N024028/1. The work at the University of Warwick was also funded by EPSRC, UK through Grant No. EP/T005963/1.

* matjaz.gomilsek@ijs.si

† Current addresses: Faculty of Engineering and Physical Sciences, University of Southampton, Southampton SO17 1BJ, United Kingdom; Max Planck Institute for the Structure and Dynamics of Matter, Luruper Chaussee 149, 22761 Hamburg, Germany

- [1] S. Li, X. Wang, and T. Rasing, Magnetic skyrmions: Basic properties and potential applications, *Interdiscip. Mater.* **2**, 260 (2023).
- [2] J. Khatua, B. Sana, A. Zorko, M. Gomilšek, K. Sethupathi, M. R. Rao, M. Baenitz, B. Schmidt, and P. Khuntia, Experimental signatures of quantum and topological states in frustrated magnetism, *Phys. Rep.* **1041**, 1 (2023).
- [3] T. Lancaster, Skyrmions in magnetic materials, *Contemp. Phys.* **60**, 246 (2019).
- [4] D. Morikawa, K. Shibata, N. Kanazawa, X. Z. Yu, and Y. Tokura, Crystal chirality and skyrmion helicity in MnSi and (Fe, Co)Si as determined by transmission electron microscopy, *Phys. Rev. B* **88**, 024408 (2013).
- [5] T. Kurumaji, T. Nakajima, M. Hirschberger, A. Kikkawa, Y. Yamasaki, H. Sagayama, H. Nakao, Y. Taguchi, T. H. Arima, and Y. Tokura, Skyrmion lattice with a giant topological hall effect in a frustrated triangular-lattice magnet, *Science* **365**, 914 (2019).
- [6] M. Hirschberger, T. Nakajima, M. Kriener, T. Kurumaji, L. Spitz, S. Gao, A. Kikkawa, Y. Yamasaki, H. Sagayama, H. Nakao, S. Ohira-Kawamura, Y. Taguchi, T. H. Arima, and Y. Tokura, High-field depinned phase and planar Hall effect in the skyrmion host Gd_2PdSi_3 , *Phys. Rev. B* **101**, 220401(R) (2020).
- [7] M. Hirschberger, L. Spitz, T. Nomoto, T. Kurumaji, S. Gao, J. Masell, T. Nakajima, A. Kikkawa, Y. Yamasaki, H. Sagayama, H. Nakao, Y. Taguchi, R. Arita, T. H. Arima, and Y. Tokura, Topological Nernst effect of the two-dimensional skyrmion lattice, *Phys. Rev. Lett.* **125**, 076602 (2020).
- [8] H. Zhang, Q. Huang, L. Hao, J. Yang, K. Noordhoek, S. Pandey, H. Zhou, and J. Liu, Anomalous magnetoresistance in centrosymmetric skyrmion-lattice magnet Gd_2PdSi_3 , *New J. Phys.* **22**, 083056 (2020).
- [9] S. Spachmann, A. Elghandour, M. Frontzek, W. Löser,

- and R. Klingeler, Magnetoelastic coupling and phases in the skyrmion lattice magnet Gd_2PdSi_3 discovered by high-resolution dilatometry, *Phys. Rev. B* **103**, 184424 (2021).
- [10] J. A. M. Paddison, B. K. Rai, A. F. May, S. Calder, M. B. Stone, M. D. Frontzek, and A. D. Christianson, Magnetic interactions of the centrosymmetric skyrmion material Gd_2PdSi_3 , *Phys. Rev. Lett.* **129**, 137202 (2022).
- [11] J. Ju, H. Saito, T. Kurumaji, M. Hirschberger, A. Kikkawa, Y. Taguchi, T. H. Arima, Y. Tokura, and T. Nakajima, Polarized neutron scattering study of the centrosymmetric skyrmion host material Gd_2PdSi_3 , *Phys. Rev. B* **107**, 024405 (2023).
- [12] K. K. Kolincio, M. Hirschberger, J. Masell, T. H. Arima, N. Nagaosa, and Y. Tokura, Kagome lattice promotes chiral spin fluctuations, *Phys. Rev. Lett.* **130**, 136701 (2023).
- [13] T. Nakajima, H. Saito, N. Kobayashi, T. Kawasaki, T. Nakamura, H. Kawano-Furukawa, S. Asai, and T. Masuda, Polarized and unpolarized neutron scattering for magnetic materials at the triple-axis spectrometer PONTA in JRR-3, *J. Phys. Soc. Jpn.* **93**, 091002 (2024).
- [14] Y. Dong, Y. Arai, K. Kuroda, M. Ochi, N. Tanaka, Y. Wan, M. D. Watson, T. K. Kim, C. Cacho, M. Hashimoto, D. Lu, Y. Aoki, T. D. Matsuda, and T. Kondo, Fermi surface nesting driving the RKKY interaction in the centrosymmetric skyrmion magnet Gd_2PdSi_3 , *Phys. Rev. Lett.* **133**, 016401 (2024).
- [15] D. Mayoh, A. Štefančič, M. Lees, and G. Balakrishnan, Crystal growth of the $R_2\text{PdSi}_3$ (R = rare earth) materials using the optical floating zone technique, *J. Cryst. Growth* **642**, 127774 (2024).
- [16] M. Hirschberger, T. Nakajima, S. Gao, L. Peng, A. Kikkawa, T. Kurumaji, M. Kriener, Y. Yamasaki, H. Sagayama, H. Nakao, *et al.*, Skyrmion phase and competing magnetic orders on a breathing kagomé lattice, *Nat. Commun.* **10**, 5831 (2019).
- [17] M. Hirschberger, S. Hayami, and Y. Tokura, Nanometric skyrmion lattice from anisotropic exchange interactions in a centrosymmetric host, *New J. Phys.* **23**, 023039 (2021).
- [18] M. O. Ogunbunmi, H. S. Nair, and A. M. Strydom, Magnetic frustration-driven ground state properties of rare-earth magnetic ions on a breathing kagome lattice: a review of the $\text{Gd}_3\text{Ru}_4\text{Al}_{12}$ structure type magnets, *Crit. Rev. Solid State Mater. Sci.* **48**, 480 (2023).
- [19] N. D. Khanh, T. Nakajima, X. Yu, S. Gao, K. Shibata, M. Hirschberger, Y. Yamasaki, H. Sagayama, H. Nakao, L. Peng, *et al.*, Nanometric square skyrmion lattice in a centrosymmetric tetragonal magnet, *Nat. Nanotechnol.* **15**, 444 (2020).
- [20] Y. Yasui, C. J. Butler, N. D. Khanh, S. Hayami, T. Nomoto, T. Hanaguri, Y. Motome, R. Arita, T. H. Arima, Y. Tokura, *et al.*, Imaging the coupling between itinerant electrons and localised moments in the centrosymmetric skyrmion magnet GdRu_2Si_2 , *Nat. Commun.* **11**, 5925 (2020).
- [21] N. D. Khanh, T. Nakajima, S. Hayami, S. Gao, Y. Yamasaki, H. Sagayama, H. Nakao, R. Takagi, Y. Motome, Y. Tokura, T. H. Arima, and S. Seki, Zoology of multiple- q spin textures in a centrosymmetric tetragonal magnet with itinerant electrons, *Adv. Sci.* **9**, 2105452 (2022).
- [22] N. Matsuyama, T. Nomura, S. Imajo, T. Nomoto, R. Arita, K. Sudo, M. Kimata, N. D. Khanh, R. Takagi, Y. Tokura, S. Seki, K. Kindo, and Y. Kohama, Quantum oscillations in the centrosymmetric skyrmion-hosting magnet GdRu_2Si_2 , *Phys. Rev. B* **107**, 104421 (2023).
- [23] G. D. A. Wood, D. D. Khalyavin, D. A. Mayoh, J. Bouaziz, A. E. Hall, S. J. R. Holt, F. Orlandi, P. Manuel, S. Blügel, J. B. Staunton, O. A. Petrenko, M. R. Lees, and G. Balakrishnan, Double- q ground state with topological charge stripes in the centrosymmetric skyrmion candidate GdRu_2Si_2 , *Phys. Rev. B* **107**, L180402 (2023).
- [24] S. Eremeev, D. Glazkova, G. Poelchen, A. Kraiker, K. Ali, A. Tarasov, S. Schulz, K. Kliemt, E. Chulkov, V. Stolyarov, *et al.*, Insight into the electronic structure of the centrosymmetric skyrmion magnet GdRu_2Si_2 , *Nanoscale Adv.* **5**, 6678 (2023).
- [25] J. Spethmann, N. D. Khanh, H. Yoshimochi, R. Takagi, S. Hayami, Y. Motome, R. Wiesendanger, S. Seki, and K. von Bergmann, SP-STM study of the multi- Q phases in GdRu_2Si_2 , *Phys. Rev. Mater.* **8**, 064404 (2024).
- [26] Y. Dong, Y. Kinoshita, M. Ochi, R. Nakachi, R. Higashinaka, S. Hayami, Y. Wan, Y. Arai, S. Huh, M. Hashimoto, *et al.*, Magnetic-domain-dependent pseudogap induced by Fermi surface nesting in a centrosymmetric skyrmion magnet, arXiv preprint (2023), arXiv:2307.08000 [cond-mat.mtrl-sci].
- [27] J. A. Paddison, J. Bouaziz, A. F. May, Q. Zhang, S. Calder, D. Abernathy, J. B. Staunton, S. Blügel, and A. D. Christianson, Spin dynamics of the centrosymmetric skyrmion material GdRu_2Si_2 , arXiv preprint (2024), arXiv:2406.04524 [cond-mat.str-el].
- [28] B. Huddart, A. Hernández-Melián, G. Wood, D. Mayoh, M. Gomilšek, Z. Guguchia, C. Wang, S. Blundell, G. Balakrishnan, and T. Lancaster, Field-orientation-dependent magnetic phases in GdRu_2Si_2 probed with muon-spin spectroscopy, arXiv preprint (2024), arXiv:2403.09431 [cond-mat.str-el].
- [29] H. Yoshimochi, R. Takagi, J. Ju, N. Khanh, H. Saito, H. Sagayama, H. Nakao, S. Itoh, Y. Tokura, T. Arima, *et al.*, Multistep topological transitions among meron and skyrmion crystals in a centrosymmetric magnet, *Nat. Phys.* **20**, 1001 (2024).
- [30] R. Takagi, N. Matsuyama, V. Ukleev, L. Yu, J. S. White, S. Francoual, J. R. Mardegan, S. Hayami, H. Saito, K. Kaneko, *et al.*, Square and rhombic lattices of magnetic skyrmions in a centrosymmetric binary compound, *Nat. Commun.* **13**, 1472 (2022).
- [31] T. Shang, Y. Xu, D. J. Gawryluk, J. Z. Ma, T. Shiroka, M. Shi, and E. Pomjakushina, Anomalous hall resistivity and possible topological hall effect in the EuAl_4 antiferromagnet, *Phys. Rev. B* **103**, L020405 (2021).
- [32] X. Y. Zhu, H. Zhang, D. J. Gawryluk, Z. X. Zhen, B. C. Yu, S. L. Ju, W. Xie, D. M. Jiang, W. J. Cheng, Y. Xu, M. Shi, E. Pomjakushina, Q. F. Zhan, T. Shiroka, and T. Shang, Spin order and fluctuations in the EuAl_4 and EuGa_4 topological antiferromagnets: A μSR study, *Phys. Rev. B* **105**, 014423 (2022).
- [33] T. Okubo, S. Chung, and H. Kawamura, Multiple- q states and the skyrmion lattice of the triangular-lattice heisenberg antiferromagnet under magnetic fields, *Phys. Rev. Lett.* **108**, 017206 (2012).
- [34] A. Leonov and M. Mostovoy, Multiply periodic states and isolated skyrmions in an anisotropic frustrated magnet, *Nat. Commun.* **6**, 8275 (2015).

- [35] V. Lohani, C. Hickey, J. Masell, and A. Rosch, Quantum skyrmions in frustrated ferromagnets, *Phys. Rev. X* **9**, 041063 (2019).
- [36] J. Pang, X. Niu, H. J. Zhao, Y. Zhang, and L. Bellaiche, Unravelling spontaneous Bloch-type skyrmion in centrosymmetric two-dimensional magnets, arXiv preprint (2023), arXiv:2312.00423 [cond-mat.mtrl-sci].
- [37] J. Bouaziz, E. Mendive-Tapia, S. Blügel, and J. B. Staunton, Fermi-surface origin of skyrmion lattices in centrosymmetric rare-earth intermetallics, *Phys. Rev. Lett.* **128**, 157206 (2022).
- [38] R. Ozawa, S. Hayami, and Y. Motome, Zero-field skyrmions with a high topological number in itinerant magnets, *Phys. Rev. Lett.* **118**, 147205 (2017).
- [39] S. Hayami, R. Ozawa, and Y. Motome, Effective bilinear-biquadratic model for noncoplanar ordering in itinerant magnets, *Phys. Rev. B* **95**, 224424 (2017).
- [40] S. Hayami and Y. Motome, Square skyrmion crystal in centrosymmetric itinerant magnets, *Phys. Rev. B* **103**, 024439 (2021).
- [41] S. Hayami, Multiple skyrmion crystal phases by itinerant frustration in centrosymmetric tetragonal magnets, *J. Phys. Soc. Japan* **91**, 023705 (2022).
- [42] S. Hayami, Anisotropic skyrmion crystal on a centrosymmetric square lattice under an in-plane magnetic field, arXiv preprint (2023), arXiv:2312.01542 [cond-mat.str-el].
- [43] T. Nomoto, T. Koretsune, and R. Arita, Formation mechanism of the helical \mathbf{Q} structure in Gd-based skyrmion materials, *Phys. Rev. Lett.* **125**, 117204 (2020).
- [44] T. Nomoto and R. Arita, *Ab initio* exploration of short-pitch skyrmion materials: Role of orbital frustration, *J. Appl. Phys.* **133**, 150901 (2023).
- [45] X. Yu, W. Koshibae, Y. Tokunaga, K. Shibata, Y. Taguchi, N. Nagaosa, and Y. Tokura, Transformation between meron and skyrmion topological spin textures in a chiral magnet, *Nature* **564**, 95 (2018).
- [46] N. Kanazawa, S. Seki, and Y. Tokura, Noncentrosymmetric magnets hosting magnetic skyrmions, *Adv. Mater.* **29**, 1603227 (2017).
- [47] M. Garst, J. Waizner, and D. Grundler, Collective spin excitations of helices and magnetic skyrmions: review and perspectives of magnonics in non-centrosymmetric magnets, *J. Phys. D: Appl. Phys.* **50**, 293002 (2017).
- [48] T. Weber, D. M. Fobes, J. Waizner, P. Steffens, G. S. Tucker, M. Böhm, L. Beddrich, C. Franz, H. Gabold, R. Bewley, *et al.*, Topological magnon band structure of emergent Landau levels in a skyrmion lattice, *Science* **375**, 1025 (2022).
- [49] M. Soda, E. M. Forgan, E. Blackburn, E. Campillo, V. Ryukhtin, I. Hoffmann, A. Kikkawa, Y. Taguchi, H. Yoshizawa, and H. Kawano-Furukawa, Asymmetric slow dynamics of the skyrmion lattice in MnSi, *Nat. Phys.* **19**, 1476 (2023).
- [50] S. J. Blundell, R. De Renzi, T. Lancaster, and F. L. Pratt, *Muon Spectroscopy: An Introduction* (Oxford University Press, Oxford, 2021).
- [51] K. J. A. Franke, B. M. Huddart, T. J. Hicken, F. Xiao, S. J. Blundell, F. L. Pratt, M. Crisanti, J. A. T. Barker, S. J. Clark, A. Štefančič, M. C. Hatnean, G. Balakrishnan, and T. Lancaster, Magnetic phases of skyrmion-hosting $\text{GaV}_4\text{S}_{8-y}\text{Se}_y$ ($y = 0, 2, 4, 8$) probed with muon spectroscopy, *Phys. Rev. B* **98**, 054428 (2018).
- [52] A. Štefančič, S. H. Moody, T. J. Hicken, M. T. Birch, G. Balakrishnan, S. A. Barnett, M. Crisanti, J. S. O. Evans, S. J. R. Holt, K. J. A. Franke, P. D. Hutton, B. M. Huddart, M. R. Lees, F. L. Pratt, C. C. Tang, M. N. Wilson, F. Xiao, and T. Lancaster, Origin of skyrmion lattice phase splitting in Zn-substituted Cu_2OSeO_3 , *Phys. Rev. Mater.* **2**, 111402(R) (2018).
- [53] T. J. Hicken, S. J. R. Holt, K. J. A. Franke, Z. Hawkhead, A. Štefančič, M. N. Wilson, M. Gomilšek, B. M. Huddart, S. J. Clark, M. R. Lees, F. L. Pratt, S. J. Blundell, G. Balakrishnan, and T. Lancaster, Magnetism and néel skyrmion dynamics in $\text{GaV}_4\text{S}_{8-y}\text{Se}_y$, *Phys. Rev. Res.* **2**, 032001(R) (2020).
- [54] T. J. Hicken, M. N. Wilson, K. J. A. Franke, B. M. Huddart, Z. Hawkhead, M. Gomilšek, S. J. Clark, F. L. Pratt, A. Štefančič, A. E. Hall, M. Ciomaga Hatnean, G. Balakrishnan, and T. Lancaster, Megahertz dynamics in skyrmion systems probed with muon-spin relaxation, *Phys. Rev. B* **103**, 024428 (2021).
- [55] M. N. Wilson, T. J. Hicken, M. Gomilšek, A. Štefančič, G. Balakrishnan, J. C. Loudon, A. C. Twitchett-Harrison, F. L. Pratt, M. Telling, and T. Lancaster, Spin dynamics in bulk MnNiGa and $\text{Mn}_{1.4}\text{Pt}_{0.9}\text{Pd}_{0.1}\text{Sn}$ investigated by muon spin relaxation, *Phys. Rev. B* **104**, 134414 (2021).
- [56] T. J. Hicken, M. N. Wilson, S. J. R. Holt, R. Khasanov, M. R. Lees, R. Gupta, D. Das, G. Balakrishnan, and T. Lancaster, Magnetism in the Néel-skyrmion host GaV_4S_8 under pressure, *Phys. Rev. B* **105**, 134414 (2022).
- [57] T. Hicken, M. Wilson, Z. Salman, T. Prokscha, A. Suter, F. Pratt, S. Zhang, G. van der Laan, T. Hesjedal, and T. Lancaster, Depth-dependent magnetic crossover in a room-temperature skyrmion-hosting multilayer, arXiv preprint (2022), arXiv:2210.06070 [cond-mat.str-el].
- [58] See Supplemental Material for details on crystal synthesis and characterization, AC susceptibility measurements, muon spectroscopy measurements (including field-dependent measurements), linear spin wave theory, *ab initio* (DFT) muon-site determination, and symmetry analysis of magnetic fields at the muon site. This includes Refs. [1, 5–7, 10, 15, 37, 50, 51, 59, 60, 71 ? ? ? ? ?].
- [59] D. Beeman and P. Pincus, Nuclear Spin-Lattice Relaxation in Magnetic Insulators, *Phys. Rev.* **166**, 359 (1968).
- [60] N. Janša, A. Zorko, M. Gomilšek, M. Pregelj, K. W. Krämer, D. Biner, A. Biffin, C. Rüegg, and M. Klanjšek, Observation of two types of fractional excitation in the Kitaev honeycomb magnet, *Nat. Phys.* **14**, 786 (2018).
- [61] J. Jensen and A. R. Mackintosh, *Rare Earth Magnetism: Structures and Excitations* (Oxford University Press, 1991).
- [62] M. Mochizuki, Spin-wave modes and their intense excitation effects in skyrmion crystals, *Phys. Rev. Lett.* **108**, 017601 (2012).
- [63] X. Xing, Y. Zhou, and H. B. Braun, Magnetic skyrmion tubes as nonplanar magnonic waveguides, *Phys. Rev. Appl.* **13**, 034051 (2020).
- [64] M. D. Frontzek, *Magnetic properties of $R_2\text{PdSi}_3$ ($R = \text{heavy rare earth}$) compounds*, PhD thesis, Technische Universität Dresden, Dresden, Germany (2009).
- [65] M. Frontzek, A. Kreyssig, M. Doerr, M. Rotter, G. Behr, W. Löser, I. Mazilu, and M. Loewenhaupt, Magnetocrystalline anisotropy in $R_2\text{PdSi}_3$ ($R = \text{Tb, Dy, Ho, Er, Tm}$) single crystals, *J. Magn. Magn. Mater.* **301**, 398 (2006).

- [66] S. Sarkar, R. Pathak, A. Delin, O. Eriksson, and V. Borisov, Unveiling mysteries of GdRu_2Si_2 : The impact of interlayer coupling on the magnetic response, arXiv preprint (2024), [arXiv:2409.06736](https://arxiv.org/abs/2409.06736) [[cond-mat.mtrl-sci](https://arxiv.org/abs/2409.06736)].
- [67] A. Garnier, D. Gignoux, D. Schmitt, and T. Shigeoka, Giant magnetic anisotropy in tetragonal GdRu_2Ge_2 and GdRu_2Si_2 , *Phys. B: Condens. Matter.* **222**, 80 (1996).
- [68] A. Garnier, D. Gignoux, N. Iwata, D. Schmitt, T. Shigeoka, and F. Zhang, Anisotropic metamagnetism in GdRu_2Si_2 , *J. Magn. Magn. Mater.* **140**, 899 (1995).
- [69] S. Jia, S. Bud'ko, G. Samolyuk, and P. Canfield, Nearly ferromagnetic Fermi-liquid behaviour in $\text{YFe}_2\text{Zn}_{20}$ and high-temperature ferromagnetism of $\text{GdFe}_2\text{Zn}_{20}$, *Nat. Phys.* **3**, 334 (2007).
- [70] P. Kotsanidis, J. Yakinthos, and E. Gamari-Seale, Magnetic properties of the ternary rare earth silicides $R_2\text{PdSi}_3$ ($R = \text{Pr, Nd, Gd, Tb, Dy, Ho, Er, Tm}$ and Y), *J. Magn. Magn. Mater.* **87**, 199 (1990).
- [71] F. Tang, M. Frontzek, J. Dshemuchadse, T. Leisegang, M. Zschornak, R. Mitrach, J.-U. Hoffmann, W. Löser, S. Gemming, D. C. Meyer, and M. Loewenhaupt, Crystallographic superstructure in $R_2\text{PdSi}_3$ compounds ($R = \text{heavy rare earth}$), *Phys. Rev. B* **84**, 104105 (2011).

Supplemental Material: Anisotropic Skyrmion and Multi- q Spin Dynamics in Centrosymmetric Gd_2PdSi_3

M. Gomilšek,^{1,2,3,*} T. J. Hicken,^{4,3} M. N. Wilson,^{5,3} K. J. A. Franke,^{6,3} B. M. Huddart,^{7,3} A. Štefančič,⁸ S. J. R. Holt,^{8,†} G. Balakrishnan,⁸ D. A. Mayoh,⁸ M. T. Birch,^{9,10,3} S. H. Moody,^{11,3} H. Luetkens,⁴ Z. Guguchia,⁴ M. T. F. Telling,¹² P. J. Baker,¹² S. J. Clark,³ and T. Lancaster³

¹Jožef Stefan Institute, Jamova c. 39, SI-1000 Ljubljana, Slovenia

²Faculty of Mathematics and Physics, University of Ljubljana, Jadranska u. 19, SI-1000 Ljubljana, Slovenia

³Department of Physics, Durham University, South Road, Durham DH1 3LE, United Kingdom

⁴Laboratory for Muon Spin Spectroscopy, Paul Scherrer Institut, 5232 Villigen PSI, Switzerland

⁵Department of Physics and Physical Oceanography, Memorial University, A1B 3X7, Canada

⁶School of Physics and Astronomy, University of Leeds, LS2 9JT, United Kingdom

⁷Clarendon Laboratory, University of Oxford, Department of Physics, Oxford OX1 3PU, United Kingdom

⁸University of Warwick, Department of Physics, Coventry CV4 7AL, United Kingdom

⁹Max Planck Institute for Intelligent Systems, Heisenbergstrasse 3, D-70569 Stuttgart, Germany

¹⁰RIKEN Center for Emergent Matter Science, JP-351-0198 Wako, Japan

¹¹Laboratory for Neutron Scattering and Imaging, Paul Scherrer Institut, 5232 Villigen PSI, Switzerland

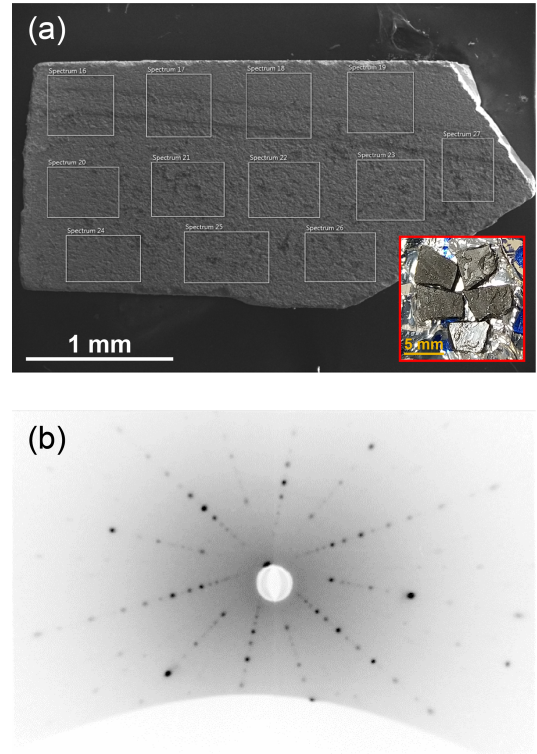
¹²ISIS Facility, STFC Rutherford Appleton Laboratory, Didcot, Oxfordshire OX11 0QX, United Kingdom

(Dated: February 4, 2025)

CRYSTAL SYNTHESIS, SEM-EDX, AND LAUE X-RAY MEASUREMENTS

Single-crystal sample synthesis was performed at the University of Warwick via the optical floating zone technique [1]. Firstly, polycrystalline buttons of Gd_2PdSi_3 were synthesised by arc melting stoichiometric quantities of Gd (99.9%, STREM), Pd (99.9%, STREM), and Si (99.999%, Sigma-Aldrich). The buttons produced were flipped and remelted several times to ensure homogeneity. After the polycrystalline buttons were formed, they were recast into a rod for single-crystal growth. Single crystals of Gd_2PdSi_3 were then grown using a four-mirror optical image furnace (equipped with four xenon arc lamps). The crystals were grown in a high purity (6N) argon atmosphere. Crystal growth was carried out using a range of growth rates, from 8 to 12 mm/h, while the feed and seed rods were counter-rotated at speeds ranging from 10 to 20 rpm. This process yielded a single-crystal boule from which plate-like samples were extracted.

Compositional analysis was performed via scanning electron microscopy (SEM) with energy-dispersive X-ray (EDX) analysis on K_α edges of Gd, Pd, and Si on a Zeiss Supra 55-VP FEGSEM [Supplementary Fig. 1(a)]. The sample stoichiometry was measured to be $\text{Gd}_{2.04(3)}\text{Pd}_{1.05(1)}\text{Si}_3$, close to the ideal Gd_2PdSi_3 . Five plate-like, $\approx 9 \text{ mm}^2 \times 0.6 \text{ mm}$ samples were extracted from the single-crystal boule and polished for muon spectroscopy (μSR) and AC susceptibility measurements [inset in Supplementary Fig. 1(a)]. Sample orientation, with the crystallographic c axis perpendicular to the plates, was checked via Laue X-ray measurements, which found a maximal deviation from perfect alignment below 4° and good sample crystallinity [Supplementary Fig. 1(b)].



Supplementary Fig. 1. (a) SEM image of an extracted Gd_2PdSi_3 single-crystal sample with marked regions from which EDX spectra were analysed. Inset: mosaic of five Gd_2PdSi_3 samples in a silver foil packet for μSR measurements. (b) Laue pattern of an isolated single-crystal sample of Gd_2PdSi_3 .

AC SUSCEPTIBILITY MEASUREMENTS

Magnetic susceptibility with magnetic field $\mathbf{H} \parallel c$ and a drive field of 1 mT at 10 Hz was measured using a Quantum Design MPMS3 at the I10 support laboratory, Diamond Light Source. The single crystal sample was fixed to a quartz rod with GE varnish. The phase diagram [Fig. 1(a) in the main text] was determined using scans of increasing field from 0 to 2 T after zero field cooling (ZFC) the sample down from 30 K to each measured temperature.

MUON SPECTROSCOPY MEASUREMENTS

Plate-like samples were assembled in a mosaic before μ SR measurements [inset in Supplementary Fig. 1(a)]. Muon data from the GPS instrument at the Swiss Muon Source (S μ S) were fit using the Gaussian and exponential models described in the main text, since a damped-cosine-oscillation model [shown as a guide to the eye in Fig. 2(a) in the main text] proved unreliable since only the first minimum of the muon polarization could be clearly resolved at early times due to strong damping of the oscillatory contribution [Fig. 2(a) in the main text], due to the broadness of the quasi-static local-field distribution at the muon site, which made separating the oscillation frequency from the Gaussian damping rate hard. An alternative Kubo–Toyabe model [2], which describes muon polarization under a broad quasi-static local-field distribution in a powder or an isotropic magnetic system, was not appropriate as our samples were anisotropic single crystals. A constant background contribution $a_{\text{bgd}} = \text{const.}$ absorbed the lack of alpha correction of detector efficiencies in some of the datasets [e.g., Fig. 2(a) in the main text], as the two are almost indistinguishable [2].

Quasi-static polarization

In ordered magnetic systems, the muon polarization at early times is dominated by quasi-static local magnetic fields at the muon site. Namely, the quasi-static muon polarization along the detector direction, which we denote z , at time t is given by [2]

$$P(t) = \int d^3\mathbf{B} p(\mathbf{B}) [\cos^2 \theta + \sin^2 \theta \cos(\gamma_\mu B t)], \quad (1)$$

where $p(\mathbf{B})$ is the probability density function that the muon at its stopping site encounters an initial quasi-static local magnetic field \mathbf{B} (i.e., the field distribution at the muon stopping site), $B = |\mathbf{B}|$, θ is the angle between the field \mathbf{B} and the detector direction z , and $\gamma_\mu = 2\pi \times 135.53 \text{ MHz/T}$ is the muon gyromagnetic ratio.

The muon asymmetry is related to the muon polarization by $A(t) = a_s P(t) + A_{\text{bgd}}(t)$, where a_s is the total sample asymmetry, and $A_{\text{bgd}}(t)$ is the background asymmetry due to muons missing the sample and hitting the sample holder [e.g., $A_{\text{bgd}}(t) = a_{\text{bgd}} = \text{const.}$ in zero field (ZF)].

When the field distribution $p(\mathbf{B})$ allows for different field magnitudes B , the oscillating term in Eq. (1) averages out to zero at late times, leaving the muons with a finite late-time asymmetry a_r (called the relaxing asymmetry) that can only relax dynamically. Its value can be calculated to be

$$a_r = a_s \langle \hat{B}_z^2 \rangle, \quad (2)$$

where $\hat{\mathbf{B}} = \mathbf{B}/B$ is the normalized initial quasi-static local-field direction at the muon site, and $\langle \dots \rangle$ is the expectation value under the field distribution $p(\mathbf{B})$.

Often one models the true quasi-static muon polarization in Eq. (1) with a damped-cosine-oscillation model

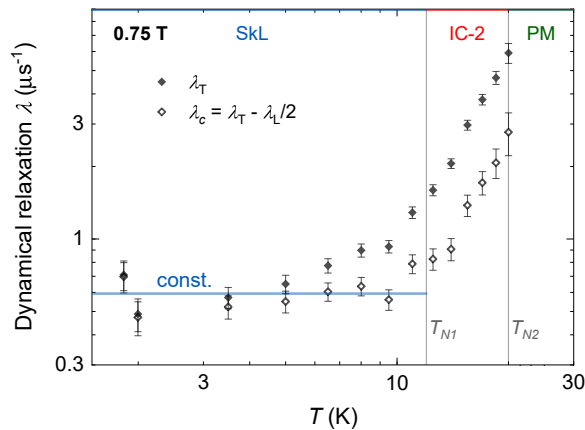
$$P(t) = (1 - p_r) \cos(\gamma_\mu B^* t) e^{-\sigma^{*2} t^2} + p_r, \quad (3)$$

where $p_r = a_r/a_s$ is the relaxing polarization [Eq. (2)], B^* is the oscillation field (related to the oscillation angular frequency $\omega = \gamma_\mu B^*$), and σ^* is the Gaussian damping rate. Both this model and the true polarization [Eq. (1)] have the same initial value $P(0) = 1$ and slope $P'(0) = 0$, while matching their initial second derivatives $P''(0)$ gives

$$\frac{2\sigma^{*2}}{\gamma_\mu^2} = \frac{\langle B_x^2 + B_y^2 \rangle}{\langle \hat{B}_x^2 + \hat{B}_y^2 \rangle} - B^{*2} = \frac{\langle B^2 \rangle - \langle B_z^2 \rangle}{1 - \langle \hat{B}_z^2 \rangle} - B^{*2}, \quad (4)$$

where x and y are axes perpendicular to the detector direction z .

Fitting the oscillation field B^* in the damped-cosine-oscillation model Eq. (3) gives $B^* \approx \langle B \rangle$, while the Gaussian model from the main text corresponds to fixing $B^* = 0$. In the fitted-damped-cosine-oscillation-model case (with $B^* \approx \langle B \rangle$), the Gaussian damping rate in Eq. (4), which we denote $\sigma' = \sigma^*$, corresponds to a weighted width of the quasi-static local-field distribution $p(\mathbf{B})$ at the muon site. For example, for an isotropic local-field distribution (e.g., in a powder), we would obtain $\sigma' \approx (\gamma_\mu/\sqrt{2}) \sqrt{\langle B^2 \rangle - \langle B \rangle^2}$, i.e., a constant times the standard-deviation (SD) width of the distribution of local-field magnitudes [2]. On the other hand, in the Gaussian model from the main text (with $B^* = 0$), the damping rate in Eq. (4), which we now denote $\sigma = \sigma^*$, corresponds to a weighted average strength of quasi-static local fields. For example, for an isotropic local-field distribution, we would obtain $\sigma = (\gamma_\mu/\sqrt{2}) \sqrt{\langle B^2 \rangle}$, i.e., the root mean square (RMS) of local-field magnitudes [2].



Supplementary Fig. 2. Comparison of the raw T-direction (*ab*-plane) dynamical muon relaxation rate from TF measurements (solid symbols) and the extracted relaxation rate due to out-of-plane (*c*-axis) spin fluctuations (unfilled symbols) in the SkL and IC-2 phases in a 0.75 T applied field.

Dynamical relaxation

At late times, exponential decay of muon polarization was observed [Fig. 2(a) in the main text]. In general, at late times, dynamical fluctuations of the local magnetic field $\mathbf{B}(t)$ at the muon site, which are described by the field-field autocorrelation function $\Phi_{\alpha\beta}(t) = \gamma_\mu^2 \langle \delta B_\alpha(t) \delta B_\beta(0) \rangle$ where $\delta \mathbf{B}(t) = \mathbf{B}(t) - \langle \mathbf{B} \rangle$, induce an exponential decay of the muon polarization function along the detector direction, which we again denote z with perpendicular directions x and y , with a relaxation rate given by [2]

$$\lambda = \int_0^\infty \cos(\omega_0 t) [\Phi_{xx}(t) + \Phi_{yy}(t)] dt, \quad (5)$$

where $\omega_0 = \gamma_\mu \langle B \rangle$ is the average Larmor angular frequency of the total magnetic field (applied plus internal). In other words, a component (z) of the muon spin relaxes at late times due to dynamical fluctuations of the local magnetic field in the plane perpendicular to that component (xy -plane). If we have a crystal with uniaxial symmetry along the c axis, we thus have relaxation rates $\lambda_L = 2\lambda_{ab}$ and $\lambda_T = \lambda_{ab} + \lambda_c$, for muon spin components along $z = L \parallel c$ and $z = T \perp c$ directions, respectively, where the individual relaxation-rate contributions are

$$\begin{aligned} \lambda_{ab} &= \int_0^\infty \cos(\omega_0 t) \Phi_{aa}(t) dt = \lambda_L/2, \\ \lambda_c &= \int_0^\infty \cos(\omega_0 t) \Phi_{cc}(t) dt = \lambda_T - \lambda_L/2, \end{aligned} \quad (6)$$

and uniaxial symmetry ensures that $\Phi_{aa}(t) = \Phi_{bb}(t)$. [Supplementary Fig. 2](#) shows the fitted T-direction relaxation rate λ_T from transverse-field (TF) measurements and the out-of-plane relaxation-rate contribution λ_c extracted from it via [Eq. \(6\)](#). The latter is also shown on

[Fig. 3\(a\)](#) in the main text. Where the temperatures at which λ_T and λ_L were measured did not match, λ_L was interpolated to the temperature of a given λ_T measurement before [Eq. \(6\)](#) was applied.

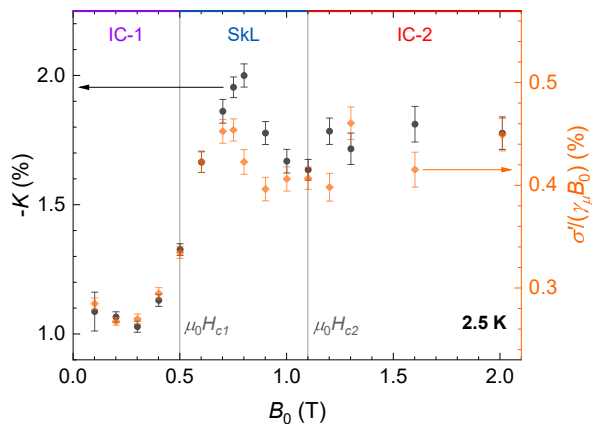
Linear spin-wave theory

At low T , the dynamical relaxation rate under the spin-wave approximation for a single magnon band due to the two-magnon (Raman) process, which is expected the dominant one in relaxing the muon spin [3], is given by [3, 4]

$$\lambda \propto \int g^2(E) f(E) [1 + f(E)] dE \propto T^p e^{-\Delta/T}, \quad (7)$$

with $p = 2D/s - 1$ [[Eq. \(1\)](#) in the main text], where $D \leq 3$ is the (integer) dimensionality of spin-wave excitations with a spin density of states $g(E)$ at energy $E \propto \omega$, s is the dominant power in their dispersion relation $E - k_B \Delta \propto |\mathbf{q} - \mathbf{q}_0|^s$ around the ordering wave vector \mathbf{q}_0 , Δ is the magnon gap, $f(E) = 1/[\exp(\beta E) - 1]$ is the Bose-Einstein distribution function, $\beta = 1/(k_B T)$, and k_B is the Boltzmann constant. Note that [Eq. \(7\)](#) is formally only valid for $p > 0$ [4]. When the magnons are gapless ($\Delta = 0$) we recover power-law behaviour, $\lambda \propto T^p$, from the main text.

Note that [Eq. \(7\)](#) is valid in all detector directions, up to a T -independent prefactor, i.e., we expect $\lambda_{ab} \propto \lambda_c \propto \lambda$ at low T in the single-magnon-band approximation. One can see this by observing that in the low- T linear spin wave theory approximation (where we expand all operators up to second order in magnon creation and annihilation operators), thermal expectation values of all spin observables, including directional relaxation-rate contributions, can only be proportional to a weighted sum of T -dependent expectation values of magnon occupation numbers $\langle n_i(\mathbf{q}) \rangle(T)$ [5], where \mathbf{q} is the wave vector and $i = 1, \dots, N$ is the magnon band index. Furthermore, only \mathbf{q} near the minima of the corresponding lowest magnon bands contribute, as muons are only sensitive to low-frequency spin fluctuations [2]. If there is only a single magnon band, $N = 1$, all spin observables thus become proportional to just one $\langle n(\mathbf{q}) \rangle(T)$ over a narrow range of \mathbf{q} , which implies that, to a good approximation, we must have $\lambda_{ab} \propto \lambda_c$ as a function of T . Note that the same holds true for general single- q spin structures, despite them appearing to exhibit up to three bands in the laboratory reference frame, as they are just single-magnon-band states from the point of view of a co-rotating reference frame [5]. On the other hand, if we have multiple truly distinct magnon bands, as we do in multi- q spin structures, multiple distinct $\langle n_i(\mathbf{q}) \rangle(T)$ can contribute with different weights to λ_{ab} and to λ_c . It thus becomes possible that $\lambda_{ab} \not\propto \lambda_c$, provided that the dominant $\langle n_i(\mathbf{q}) \rangle(T)$ contributions are sufficiently different,



Supplementary Fig. 3. Field dependence of the muon Knight shift (black), and the distribution width of quasi-static local fields at the muon site normalized by the applied field (orange), at $T = 2.5$ K under TF. Vertical lines highlight the critical fields.

i.e., that the spin state is sufficiently anisotropic. An example of this is seen in the main text in the anisotropic multi- q SkL and IC-1 phases [Figs. 3(a) and 2(c) in the main text, respectively].

Field dependence

We performed field-dependent TF μ SR measurements at a base $T = 2.5$ K on the HAL-9500 instrument at the S μ S. In contrast to GPS measurements, the initial muon spin orientation pointed at an angle of $\theta \approx 90^\circ$ from the c axis [see Fig. 1(b) in the main text] to maximize the number of muon decays measured by detectors along the T direction. Early-time T-direction data were fitted using a model consisting of a sum of two damped oscillations, $A(t) = a_s \cos(\omega t + \varphi) e^{-\sigma'^2 t^2} + a_{\text{bgd}} \cos(\omega_0 t + \varphi_0)$, the first due to the sample, and the second due to the silver background. Here, the fitted silver-background angular frequency ω_0 gave an estimate of the applied magnetic field $B_0 = \mu_0 H = \omega_0 / \gamma_\mu$, whereas the fitted sample angular frequency ω yielded the average magnitude of the local magnetic field $\langle B \rangle = \omega / \gamma_\mu$ at the muon site (see section Quasi-static polarization). From these, the local muon Knight shift was calculated as $K = (\langle B \rangle - B_0) / B_0 = \omega / \omega_0 - 1$ [2]. Note that the sample contribution to the muon asymmetry in this model follows Eq. (3) with the usual TF approximation $p_r \approx 0$ [2]. The latter can be justified when the applied TF field, which points along c , is much larger than internal fields components parallel to the detector direction $z = \mathbf{T} \perp c$, and hence also when $|K| \ll 1$, which results in $\langle \hat{B}_c^2 \rangle \approx 1$ and thus $p_r = \langle \hat{B}_z^2 \rangle \leq 1 - \langle \hat{B}_c^2 \rangle \approx 0$ via Eq. (2).

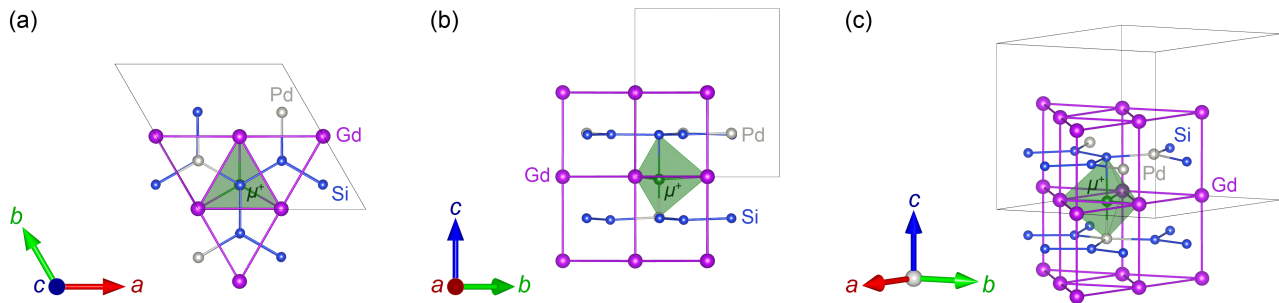
The obtained muon Knight shift (which is indeed much smaller than 100%, justifying the model we used) is shown in Supplementary Fig. 3, alongside the local-field

distribution width σ' / γ_μ [Eq. (4)] divided by the applied field B_0 . The obtained critical applied fields $\mu_0 H_{c1} = 0.5(1)$ T and $\mu_0 H_{c2} = 1.1(1)$ T are consistent with AC susceptibility [Fig. 1(a) in the main text] [6–8]. We see that in the IC-1 and IC-2 phases $K \propto \sigma' / B_0 \approx \text{const.}$, which implies $B - B_0 \propto \sigma' \propto B_0$ (i.e., the local average magnetization is proportional to the width of the local-magnetic-field distribution, which is also approximately proportional to the applied magnetic field). On the other hand, $K \not\propto \sigma' / B_0 \neq \text{const.}$ in the SkL phase, with both quantities showing clear peaks for applied fields near the middle of the phase. A similar peak in quasi-static magnetism is also observed in other SkL hosts near the middle of their SkL phases [9] (e.g., in noncentrosymmetric GaV₄S₈ and GaV₄Se₈ as a function of T). However, intriguingly, the peaks of K and σ' / B_0 in Gd₂PdSi₃ appear to be slightly shifted in field relative to each other, with the one in K appearing at 0.70(5) T and the one in σ' / B_0 appearing at 0.80(5) T.

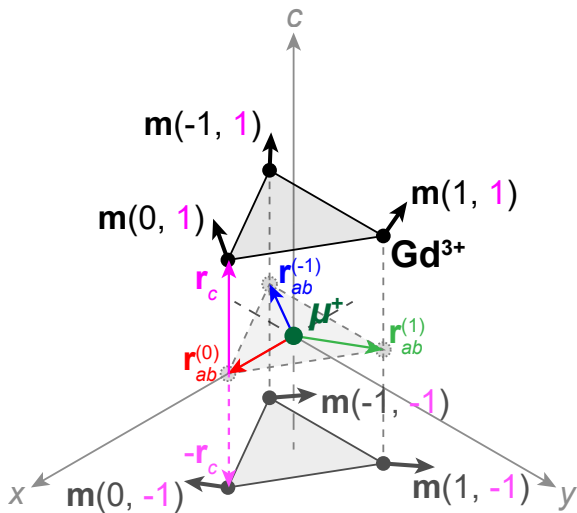
AB INITIO MUON SITE CALCULATIONS

Muon stopping sites were determined using the MuFinder program [10], which was used to run, cluster, and analyse the results of *ab initio* muon-stopping-site calculations performed using the CASTEP density functional theory (DFT) software [11]. For these, we used the PBE exchange–correlation functional [12] and ultra-soft pseudopotentials. Gd₂PdSi₃ forms a centrosymmetric superstructure with ABCDBADC stacking of inter-layer Pd and Si atomic configurations [6, 13]. Muon sites were calculated in a reduced superstructure with just two Pd/Si layers in the two most common layer stackings: AB and CD, as these two stackings already account for 50% of pairwise Pd/Si layer combinations in the full superstructure. The reduced unit cell dimensions of $8.16 \times 8.16 \times 8.19 \text{ \AA}^3$ were still large enough to avoid finite-size effects around the implanted muon. A 490 eV plane-wave energy cutoff and $2 \times 2 \times 2$ Monkhorst–Pack grid [14] reciprocal-space sampling was chosen to achieve DFT convergence. Total energies were converged to within 10^{-5} eV/atom in the self-consistent field (SCF) DFT loop, while muon-site geometry was converged to within a maximum force tolerance of 0.05 eV/Å on both the muon and the nuclei.

In all of the considered local stacking configurations, muons were found to occupy the same symmetric position at the centre of an ab -plane Gd³⁺ triangle (Supplementary Fig. 4), with only a small displacement of -0.29 and $+0.14$ Å along the out-of-plane (c -axis) direction under AB and CD Pd/Si layer stacking, respectively. Due to the similarity between the stackings, we expect that all Gd³⁺ layers in Gd₂PdSi₃ host a muon site of this kind.



Supplementary Fig. 4. Lowest-energy muon (μ^+) stopping site in Gd_2PdSi_3 (green). Shown are two neighbouring hexagonal Pd/Si (gray/blue, respectively) superstructure layers C and D around a triangular ab plane of Gd^{3+} ions (purple) in which the muon stops.



Supplementary Fig. 5. Geometry of the muon site from Supplementary Fig. 4 showing the magnetic moments $\mathbf{m}(j, \pm 1)$ of the six Gd^{3+} spins discussed in the text. Here, the local x axis is defined as pointing along the $\mathbf{r}_{ab}^{(0)}$ direction.

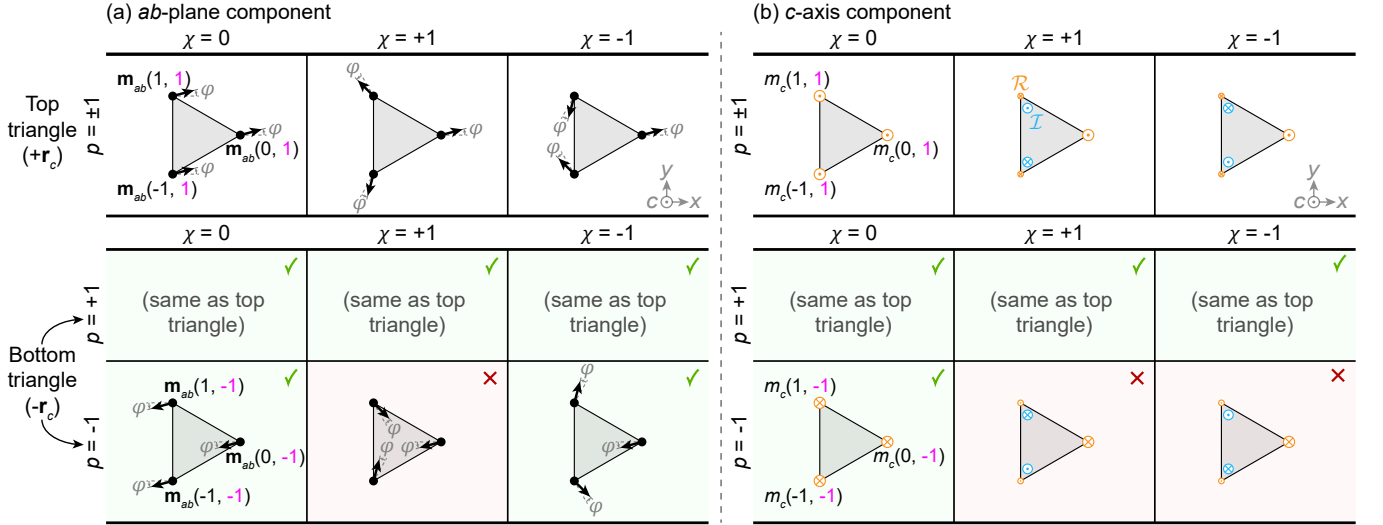
MAGNETIC FIELDS AT THE MUON SITE

Magnetic fields at the muon site in Gd_2PdSi_3 originate from Gd^{3+} spins. In this section, we will show that, to a good approximation, in-plane (ab -plane) and out-of-plane (c -axis) components of these spins generate exclusively in-plane ($\mathbf{B} \perp c$) and out-of-plane ($\mathbf{B} \parallel c$) local magnetic fields at the muon site, respectively. We will call contributions to the magnetic field at the muon site that obey this property direction-preserving, while we will call those that do not direction-mixing. We will show that direction-mixing contributions are almost negligible in Gd_2PdSi_3 due to the nature of its muon site and its magnetic state.

Firstly, effective magnetic fields from isotropic hyper-

fine contact interactions of the muon's spin with the local electron spin density (which are usually small) are all direction-preserving [2]. Secondly, dipolar fields from Gd^{3+} spins in the same ab plane as the muon are also all direction-preserving. This includes the three dominant, nearest-neighbouring (NN) Gd^{3+} spins found at a distance $r_1 = 2.35 \text{ \AA}$ from the muon, as well as the three next-nearest-neighbouring Gd^{3+} spins. Thus, the only potentially-direction-mixing magnetic fields could come from Gd^{3+} spins outside of the muon's local ab plane, with the closest being next-next-nearest-neighbouring (NNNN) Gd^{3+} spins, found at a distance $r_3 = 4.83 \text{ \AA}$ from the muon. However, these can contribute at most $(r_1/r_3)^3 = 12\%$ as much to the magnetic field at the muon site as the dominant, NN Gd^{3+} spins, just from the decrease of dipolar field strength with distance.

Moreover, the local muon-site symmetry further strongly suppresses any direction-mixing contributions from Gd^{3+} spins outside of the muon's local ab plane. Namely, ignoring atoms other than Gd, the muon site lies on both a mirror plane ab and an axis of threefold symmetry c (Supplementary Fig. 4), which causes most potentially-direction-mixing contributions to cancel at the muon position. To see this, we will consider a general sextet of Gd^{3+} spins with magnetic moments $\mathbf{m}(j, \pm 1)$ displaced from the muon by $\mathbf{r}(j, \pm 1) = \mathbf{r}_{ab}^{(j)} \pm \mathbf{r}_c$, where $\mathbf{r}_{ab}^{(j)} = R^j \mathbf{r}_{ab}^{(0)}$ is the displacement within the ab plane, R is a rotation about the $+c$ axis by 120° , $j = -1, 0, 1$, and $\pm \mathbf{r}_c$ is the displacement along the c axis (see Supplementary Fig. 5). Note that due to Gd_2PdSi_3 's crystal structure, every Gd^{3+} ion can be assigned to a unique sextet relative to the muon, and that all Gd^{3+} spins in a sextet are at equal distance from the muon. We can uniquely decompose the ab -plane and c -axis components



Supplementary Fig. 6. Symmetry-adapted decomposition [Eq. (8)] of (a) ab -plane and (b) c -axis components of magnetic moments in a sextet of Gd^{3+} spins comprised of two triangles (top and bottom) shown in Supplementary Fig. 5. At a given reflection parity p and chirality χ , the amplitude of a contribution is given by: (a) a real vector $\tilde{\mathbf{m}}_{ab}(\chi, p) = \mathbf{m}_{ab}(0, 1)$ in the ab plane, oriented at an angle φ from the $\mathbf{r}_{ab}^{(0)}$ (x -axis) direction, or (b) a complex number $\tilde{m}_c(\chi, p) = m_c(0, 1)$, here shown if real and positive. Diameters of circles on panel (b) are proportional to the real (\mathcal{R} , orange) and imaginary (\mathcal{I} , cyan) parts of complex c -axis magnetic moment contributions $m_c(j, \pm 1)$, while their positive or negative sign is indicated by a dot or a cross, respectively, inside the circle. Cell shading indicates whether the total dipolar contribution to the magnetic field at the muon site for a given p and χ is direction-preserving (green shading and check mark) or direction-mixing (red shading and cross). As argued below, direction-mixing contributions to the are strongly suppressed in Gd_2PdSi_3 .

of magnetic moments in a Gd^{3+} sextet as

$$\mathbf{m}_{ab}(j, \pm 1) = \sum_{p=1, -1} p^{(1\mp 1)/2} \sum_{\chi=-1}^1 R^{j\chi} \tilde{\mathbf{m}}_{ab}(\chi, p), \quad (8)$$

$$m_c(j, \pm 1) = \sum_{p=1, -1} p^{(1\mp 1)/2} \sum_{\chi=-1}^1 \omega^{j\chi} \tilde{m}_c(\chi, p).$$

where $\omega = e^{2\pi i/3}$ is a third root of unity, and $\tilde{\mathbf{m}}_{ab}(\chi, p)$ and $\tilde{m}_c(\chi, p)$ are ab -plane and c -axis amplitudes, respectively, of contributions with parity $p = 1, -1$ (symmetric and antisymmetric, respectively) under reflections over the muon's ab plane, and chirality $\chi = -1, 0, 1$ (negative, achiral, and positive, respectively) under threefold rotations around the muon's local c axis. Here, amplitudes $\tilde{\mathbf{m}}_{ab}(\chi, p)$ are arbitrary real vectors in the ab plane, achiral $\tilde{m}_c(0, p)$ are arbitrary real numbers, and positive-chirality $\tilde{m}_c(1, p)$ are arbitrary complex numbers. On the other hand, negative chirality amplitudes $\tilde{m}_c(-1, p) = \tilde{m}_c(1, p)^*$ are fully determined via complex conjugation * from positive chirality amplitudes $\tilde{m}_c(1, p)$, since the magnetic moments $\mathbf{m}(j, \pm 1)$ produced by Eq. (8) must be real vectors. The patterns of magnetic moments in a Gd^{3+} spin sextet in individual p and χ contributions are shown in Supplementary Fig. 6.

To see which p and χ contributions are direction-mixing, we write the dipolar magnetic field at the muon site due to a magnetic moment \mathbf{m} displaced from the

muon by \mathbf{r} as

$$\mathbf{B} = \frac{\mu_0}{4\pi r^3} \left(\frac{3}{r^2} [\mathbf{r} \otimes \mathbf{r}] \mathbf{m} - \mathbf{m} \right) \propto \frac{1}{r^3}, \quad (9)$$

where μ_0 is the vacuum permeability, $r = |\mathbf{r}|$, $\mathbf{a} \otimes \mathbf{b} = \mathbf{a} \mathbf{b}^T$ denotes the outer product of column vectors \mathbf{a} and \mathbf{b} , and T denotes a vector transpose. Here, only the first term can be direction-mixing. For a Gd^{3+} magnetic moment at position $\mathbf{r} = \mathbf{r}(j, \pm 1) = \mathbf{r}_{ab}^{(j)} \pm \mathbf{r}_c$, we can expand it as

$$\mathbf{r} \otimes \mathbf{r} = [\mathbf{r}_{ab}^{(j)} \otimes \mathbf{r}_{ab}^{(j)} + \mathbf{r}_c \otimes \mathbf{r}_c] \pm [\mathbf{r}_{ab}^{(j)} \otimes \mathbf{r}_c + \mathbf{r}_c \otimes \mathbf{r}_{ab}^{(j)}]. \quad (10)$$

Here, the terms in the first square bracket are direction-preserving, while those in the second square bracket are direction-mixing. Summing up the dipolar fields at the muon site from all Gd^{3+} spins in a sextet, we find that only antisymmetric ($p = -1$) contributions can be direction-mixing, and of those only positive-chirality ($\chi = +1$) ab -plane magnetic moments and chiral ($\chi = \pm 1$) c -axis magnetic moments are actually direction mixing. Explicitly, we find that the c -axis and ab -plane components of the magnetic field at the muon site due to direction-mixing are proportional to $|\tilde{\mathbf{m}}_{ab}(1, -1)| \cos \varphi$ and $|\tilde{m}_c(1, -1)|$, respectively, where φ is the angle between vectors $\tilde{\mathbf{m}}_{ab}(1, -1)$ and $\mathbf{r}_{ab}^{(0)}$ [see Supplementary Fig. 6(a)].

We next argue that the amplitudes of these direction-mixing contributions for Gd^{3+} spins close to the muon

site are actually negligible in Gd_2PdSi_3 . Firstly, previous studies found predominantly ferromagnetic correlations between NN Gd^{3+} layers in Gd_2PdSi_3 [15, 16], implying that $\mathbf{m}(j, 1) \approx \mathbf{m}(j, -1)$ for layers close to the muon, and thus that symmetric ($p = 1$) contributions, which are direction-preserving, dominate. We note that, as Gd^{3+} spins in a sextet are always an even number of Gd layers apart, even the presence of antiferromagnetic NN Gd layer correlations would lead to the same conclusion. In other words, only intermediate-wavelength inter-layer (c -axis) correlations could produce a direction-mixing magnetic field at the muon site. Secondly, since the ab -plane modulation wavelengths of incommensurate spin structures in Gd_2PdSi_3 are $\lambda \approx 25 \text{ \AA}$ [6, 17], and thus much larger than the nearest-neighbour Gd^{3+} -ion distance of $d_{\text{Gd-Gd}} = 4.08 \text{ \AA} \ll \lambda$ [6, 13], we expect that achiral contributions ($\chi = 0$; i.e., locally approximately-ferromagnetic), which are direction-preserving, dominate. The amplitudes of direction-mixing contributions, which are both antisymmetric ($p = -1$) and chiral ($\chi = \pm 1$) at the same time, are thus expected to be strongly suppressed in Gd_2PdSi_3 .

In summary: (i) direction-mixing contributions to the local magnetic field at the muon site can only come from far-away Gd^{3+} spins (NNNN or further, and in a different ab plane than the muon), with their dipolar fields suppressed with distance r as $(r_1/r)^3 \ll 1$, and (ii) the amplitudes of direction-mixing contributions in the local magnetic structure around the muon are strongly suppressed by the relatively-long-wavelength modulation of Gd^{3+} magnetic moments in Gd_2PdSi_3 (twice separately, both due to long wavelengths along the c -axis and within the ab -plane). We can thus safely neglect any direction-mixing contributions to the local magnetic field at the muon site in the analysis of μSR data presented in the main text.

* matjaz.gomilsek@ijs.si

† Current addresses: Faculty of Engineering and Physical Sciences, University of Southampton, Southampton SO17 1BJ, United Kingdom; Max Planck Institute for the Structure and Dynamics of Matter, Luruper Chaussee 149, 22761 Hamburg, Germany

- [1] D. Mayoh, A. Štefančič, M. Lees, and G. Balakrishnan, Crystal growth of the $R_2\text{PdSi}_3$ ($R = \text{rare earth}$) materials using the optical floating zone technique, *J. Cryst. Growth* **642**, 127774 (2024).
- [2] S. J. Blundell, R. De Renzi, T. Lancaster, and F. L. Pratt, *Muon Spectroscopy: An Introduction* (Oxford University Press, Oxford, 2021).
- [3] D. Beeman and P. Pincus, Nuclear Spin-Lattice Relaxation in Magnetic Insulators, *Phys. Rev.* **166**, 359 (1968).
- [4] N. Janša, A. Zorko, M. Gomilšek, M. Pregelj, K. W. Krämer, D. Biner, A. Biffin, C. Rüegg, and M. Klanjšek, Observation of two types of fractional excitation in the Kitaev honeycomb magnet, *Nat. Phys.* **14**, 786 (2018).
- [5] S. Toth and B. Lake, Linear spin wave theory for single-Q incommensurate magnetic structures, *J. Phys.: Condens. Matter* **27**, 166002 (2015).
- [6] T. Kurumaji, T. Nakajima, M. Hirschberger, A. Kikkawa, Y. Yamasaki, H. Sagayama, H. Nakao, Y. Taguchi, T. H. Arima, and Y. Tokura, Skyrmion lattice with a giant topological hall effect in a frustrated triangular-lattice magnet, *Science* **365**, 914 (2019).
- [7] M. Hirschberger, T. Nakajima, M. Kriener, T. Kurumaji, L. Spitz, S. Gao, A. Kikkawa, Y. Yamasaki, H. Sagayama, H. Nakao, S. Ohira-Kawamura, Y. Taguchi, T. H. Arima, and Y. Tokura, High-field depinned phase and planar Hall effect in the skyrmion host Gd_2PdSi_3 , *Phys. Rev. B* **101**, 220401(R) (2020).
- [8] M. Hirschberger, L. Spitz, T. Nomoto, T. Kurumaji, S. Gao, J. Masell, T. Nakajima, A. Kikkawa, Y. Yamasaki, H. Sagayama, H. Nakao, Y. Taguchi, R. Arita, T. H. Arima, and Y. Tokura, Topological Nernst effect of the two-dimensional skyrmion lattice, *Phys. Rev. Lett.* **125**, 076602 (2020).
- [9] K. J. A. Franke, B. M. Huddart, T. J. Hicken, F. Xiao, S. J. Blundell, F. L. Pratt, M. Crisanti, J. A. T. Barker, S. J. Clark, A. Štefančič, M. C. Hatnean, G. Balakrishnan, and T. Lancaster, Magnetic phases of skyrmion-hosting $\text{GaV}_4\text{S}_{8-y}\text{Se}_y$ ($y = 0, 2, 4, 8$) probed with muon spectroscopy, *Phys. Rev. B* **98**, 054428 (2018).
- [10] B. Huddart, A. Hernández-Melián, T. Hicken, M. Gomilšek, Z. Hawkhead, S. Clark, F. Pratt, and T. Lancaster, MuFinder: A program to determine and analyse muon stopping sites, *Comput. Phys. Commun.* **280**, 108488 (2022).
- [11] S. J. Clark, M. D. Segall, C. J. Pickard, P. J. Hasnip, M. J. Probert, K. Refson, and M. Payne, First principles methods using CASTEP, *Z. Kristall.* **220**, 567 (2005).
- [12] J. P. Perdew, K. Burke, and M. Ernzerhof, Generalized gradient approximation made simple, *Phys. Rev. Lett.* **77**, 3865 (1996).
- [13] F. Tang, M. Frontzek, J. Dshemuchadse, T. Leisegang, M. Zschornak, R. Mitrach, J.-U. Hoffmann, W. Löser, S. Gemming, D. C. Meyer, and M. Loewenhaupt, Crystallographic superstructure in $R_2\text{PdSi}_3$ compounds ($R = \text{heavy rare earth}$), *Phys. Rev. B* **84**, 104105 (2011).
- [14] H. J. Monkhorst and J. D. Pack, Special points for Brillouin-zone integrations, *Phys. Rev. B* **13**, 5188 (1976).
- [15] J. Bouaziz, E. Mendive-Tapia, S. Blügel, and J. B. Staunton, Fermi-surface origin of skyrmion lattices in centrosymmetric rare-earth intermetallics, *Phys. Rev. Lett.* **128**, 157206 (2022).
- [16] J. A. M. Paddison, B. K. Rai, A. F. May, S. Calder, M. B. Stone, M. D. Frontzek, and A. D. Christianson, Magnetic interactions of the centrosymmetric skyrmion material Gd_2PdSi_3 , *Phys. Rev. Lett.* **129**, 137202 (2022).
- [17] S. Li, X. Wang, and T. Rasing, Magnetic skyrmions: Basic properties and potential applications, *Interdiscip. Mater.* **2**, 260 (2023).